PHYSICAL REVIEW B **68**, 134305 (2003)

Temperature dependence of lattice vibrations and analysis of the specific heat of graphite

Takeshi Nihira*
Faculty of Engineering, Ibaraki University, Hitachi, Ibaraki-ken 316-8511, Japan

Tadao Iwata[†]
Japan Atomic Energy Research Institute, Tokai-mura, Naka-gun, Ibaraki-ken 319-1195, Japan

(Received 4 March 2003; published 24 October 2003)

In the semicontinuum model of lattice vibrations in graphite proposed by Komatsu and Nagamiya, the expressions of the dispersion relation contain the elastic constants C_{11}, C_{12}, C_{13}, C_{33}, C_{44}, and κ and the interlayer spacing c as parameters, where $c\rho\kappa^2$ is the bending elastic constant of a graphite layer and ρ is the density. We improve this semicontinuum model by taking these parameters as a function of temperature. For the parameters except κ, we use the experimental data already known and the relations derived from them. κ is determined by fitting the calculated specific heat to the experimental one. The experimental specific heat for single-crystal graphite is derived by evaluating the data reported in the literature. With the value of κ thus determined, the improved semicontinuum model can explain the experimental specific heat well in the temperature range below 350 K. Then, κ decreases more rapidly with increasing temperature than the other elastic constants; this result means that softening of the out-of-plane vibrations occurs. It is suggested that the softening is closely related to the negative thermal expansion parallel to the layer planes. The calculated Grüneisen constants are compared with the experimental ones. The second derivative of the specific heat curve with respect to temperature gives information on the frequency distribution function of lattice vibrations. From the analysis of the low-temperature specific heat, the value of C_{44} at room temperature is determined to be 0.425×10^{11} dyn/cm^2.

DOI: 10.1103/PhysRevB.68.134305 PACS number(s): 63.20.Dj, 65.40.Ba

I. INTRODUCTION

It is well known that the forces between the atoms in graphite are extremely anisotropic; those between adjacent basal planes are about two orders of magnitude smaller than the forces between neighboring atoms in the same plane. The strong anisotropy of the forces affects the lattice vibrations. For the lattice vibrations of graphite, a number of theoretical and experimental studies have already been made.[1–22] Of these, the semicontinuum model proposed by Komatsu and Nagamiya[1–3] is the only one that has succeeded in expressing the dispersion relation of lattice vibrations analytically. The model has been used to calculate various physical properties, such as specific heat,[1,3,23–25] thermal conductivity,[26–35] thermal expansion,[36] thermal vibration amplitudes,[37,38] elastic constants,[39] electron transport properties,[40–42] and thermoelectric power.[43]

In the semicontinuum model of graphite, the lattice vibrations are separated into three modes; the in-plane longitudinal mode, the in-plane transverse mode, and the out-of-plane mode. The expressions of the dispersion relation contain the elastic constants C_{11}, C_{12}, C_{13}, C_{33}, C_{44}, and κ and the interlayer spacing c as parameters, where $c\rho\kappa^2$ is the bending elastic constant of a graphite layer and ρ is the density. The usefulness of a lattice vibration model can be evaluated by comparing the calculated specific heat values by the model with the experimental ones. Komatsu calculated the specific heat by using the semicontinuum model with C_{33}, C_{44}, and κ as adjustable parameters and determined these parameters so as to fit the calculated values to the experimental ones for various kinds of graphite specimens below 20 K.[23,24] Thus, he showed that the semicontinuum model, with the suitable values of parameters, can well explain the specific heat below 20 K. As the temperature increases above 20 K, however, if the same parameters are used, the calculated specific heat values by the model deviate gradually from the experimental ones.

The elastic constants and the interlayer spacing change with temperature, which is due to the anharmonicity of the potential energy. As a result, the dispersion relation of lattice vibrations should change with temperature. In the present paper, we improve the semicontinuum model by taking the model parameters (i.e., the elastic constants and the interlayer spacing) as a function of temperature. Incidentally, in the Debye model of lattice vibrations in isotropic solids, the temperature dependence of the frequency distribution function is such that the Debye characteristic temperature (or the Debye frequency) changes with temperature.[44–46] For all parameters except κ, we use the experimental data already known and the relations derived from them. Since κ cannot be measured by the conventional mechanical methods, we determine it as a function of temperature by fitting the calculated specific heat values to the experimental ones.

We derive the specific heat values that are proper to single-crystal graphite by evaluating the specific heat data reported in the literature, and formulate them. The formulated data are adopted as the experimental specific heat values for fitting.

The improved semicontinuum model, if we assume the temperature dependence of κ determined in the present analysis, can explain the specific heat well in the temperature range below 350 K. The introduction of temperature dependence into the model parameters extends the temperature range in which the semicontinuum model is applicable from below 20 K to below 350 K.

The present analysis predicts that κ decreases more rapidly with increasing temperature than the other elastic constants; this means that softening of the out-of-plane vibration occurs. We suggest that the rapid decrease of κ with temperature is related to the contraction of the a spacing, i.e., the negative thermal expansion parallel to the layer planes below about 650 K. It is conceivable, however, that the inadequacy of the model results in the unusual temperature dependence of κ. Whether the predicted decrease of κ is physically valid or not should be tested by experiments, such as neutron scattering, infrared reflection, electron energy loss spectroscopy, and x-ray and neutron Bragg reflection.

In addition, we calculate the Grüneisen constants and compare them with the experimental ones. It is shown that the second derivative of the specific heat curve with respect to temperature gives information on the frequency distribution function of lattice vibrations. From the analysis of the low-temperature specific heat, the value of C_{44} at room temperature is determined to be 0.425×10^{11} dyn/cm^2.

II. THE SEMI-CONTINUUM MODEL OF KOMATSU AND NAGAMIYA

Komatsu and Nagamiya proposed the semicontinuum model of the lattice vibrations of graphite, in which the graphite crystal is assumed as an assembly of thin elastic plates equally spaced and with compressional and shearing couplings between adjacent plates.[1–3] We summarize the semicontinuum model briefly.

The lattice vibrations of graphite are almost completely separated into three kinds of modes; namely, the in-plane longitudinal mode, the in-plane transverse mode, and the out-of-plane mode. The respective dispersion relations are given by

$$\omega_l^2=v_l^2(q_x^2+q_y^2)+\frac{4\zeta}{c^2}\sin^2\left(\frac{cq_z}{2}\right), \tag{1}$$

$$\omega_t^2=v_t^2(q_x^2+q_y^2)+\frac{4\zeta}{c^2}\sin^2\left(\frac{cq_z}{2}\right), \tag{2}$$

$$\omega_c^2=\kappa^2(q_x^2+q_y^2)^2+4\mu^2\sin^2\left(\frac{cq_z}{2}\right)+\zeta(q_x^2+q_y^2), \tag{3}$$

where ω is the angular frequency, q is the wave vector, and the subscripts l, t, and c refer to the in-plane longitudinal mode, the in-plane transverse mode, and the out-of-plane mode, respectively. v_l and v_t are the wave velocities and are given by using the elastic constants C_{ij} as follows:

$$v_l=\left[\frac{1}{\rho}\left(C_{11}-\frac{C_{13}^2}{C_{33}}\right)\right]^{1/2}, \tag{4}$$

$$v_t=\left[\frac{1}{2\rho}(C_{11}-C_{12})\right]^{1/2}. \tag{5}$$

The two constants ζ and μ are related to the elastic constants C_{ij} as

$$\rho\zeta=C_{44} \tag{6}$$

and

$$c^2\rho\mu^2=C_{33}, \tag{7}$$

where ρ is the volume density and c is the interlayer spacing. $c\rho\kappa^2$ is the bending elastic constant of a graphite layer.

The frequency distribution functions (per mol) $D(\omega)$ for the two in-plane modes are derived from the dispersion relations of Eqs. (1) and (2):

$$\omega\leqslant\omega_z:\ \ D(\omega)=\frac{V}{\pi^2cv_i^2}\,\omega\sin^{-1}\left(\frac{\omega}{\omega_z}\right), \tag{8}$$

$$\omega\geqslant\omega_z:\ \ D(\omega)=\frac{V}{\pi^2cv_i^2}\,\omega\frac{\pi}{2}, \tag{9}$$

where

$$\omega_z=2\frac{\zeta^{1/2}}{c}=2\left(\frac{C_{44}}{c^2\rho}\right)^{1/2}. \tag{10}$$

The subscript i indicates l and t for the longitudinal mode and the transverse mode, respectively, and V is the molar volume.

Similarly, the frequency distribution function (per mol) for the out-of-plane mode is derived from Eq. (3):

$\omega\leqslant\omega_z'$:

$$D(\omega)=\frac{V}{2\pi^2\kappa c}\left(\frac{\omega}{\omega_z'}\right)\int_0^{\sin^{-1}\{[1+(\zeta^2/4\kappa^2\omega^2)]^{-1/2}\}}\left[1-\left(\frac{\omega}{\omega_z'}\right)^2\left(1+\frac{\zeta^2}{4\kappa^2\omega^2}\right)\sin^2\phi\right]^{-1/2}d\phi, \tag{11}$$

$\omega \geqslant \omega_z'$:

$$D(\omega) = \frac{V}{2\pi^2 \kappa c}\left(1 + \frac{\zeta^2}{4\kappa^2\omega^2}\right)^{-1/2} \times \int_0^{\pi/2}\left[1 - \left(\frac{\omega_z'}{\omega}\right)^2\left(1 + \frac{\zeta^2}{4\kappa^2\omega^2}\right)^{-1}\sin^2\phi\right]^{-1/2} d\phi, \tag{12}$$

where

$$\omega_z' = 2\mu = 2\left(\frac{C_{33}}{c^2\rho}\right)^{1/2}. \tag{13}$$

The Debye frequency ω_D for each mode is obtained from

$$\int_0^{\omega_D} D(\omega)\, d\omega = N_0, \tag{14}$$

where N_0 is Avogadro's number, $V/N_0 = (3\sqrt{3}/4)a^2 c$, and a is the nearest neighbor atomic spacing in the layer plane.

In graphite the unit cell has four atoms and therefore the lattice vibrations consist of three branches of acoustic modes and nine branches of optical modes. On the other hand, in the present semicontinuum model it is assumed that the graphite layer is a thin elastic plate and the virtual unit cell has one atom. As a result, there are three branches of vibrational modes as described above. Under the condition of Eq. (14), however, the total number of vibrational modes belonging to all the branches in the semicontinuum model is equal to that in graphite. The optical modes in graphite are treated as if they were merely elastic waves of very short wavelength in the semicontinuum model.

III. TEMPERATURE DEPENDENCE OF MODEL PARAMETERS

We improve the semicontinuum model by taking account of the temperature dependence of elastic constants and the thermal expansion. The independent model parameters, which are functions of temperature, are the elastic constants C_{11}, C_{12}, C_{13}, C_{33}, C_{44}, and κ and the interlayer spacing c. We assume that the thermal expansion in the a-axis direction can be neglected so that $c\rho$ is independent of temperature.

A. Elastic constants

Blakslee *et al.* determined five elastic constants C_{ij} at room temperature of highly oriented pyrolytic graphite (HOPG) by ultrasonic, sonic resonance, and static test methods.[47] Their results for C_{ij} except C_{44} have been widely accepted as typical of the graphite single crystal.

Reported values of C_{44} have varied considerably, depending on the specimens and the method of measurement. Blakslee *et al.* obtained C_{44} values of $(0.018-0.035) \times 10^{11}$ dyn/cm^2 at room temperature for HOPG.[47] Soule and Nezbeda observed values of $(0.013-0.166)\times 10^{11}$ dyn/cm^2 at room temperature for natural graphite single crystals by the static-shear stress strain and the ultrasonic method.[48] The C_{44} values obtained by these mechanical measurements have been considered to be much lower than the intrinsic C_{44} value because of the existence of mobile basal dislocations. Therefore, when the dislocations were pinned by doped boron atoms[48] or defects produced by neutron irradiation,[49,50] the C_{44} value at room temperature increased rapidly up to a saturation value of approximately 0.40×10^{11} dyn/cm^2. On the other hand, from the analysis of the specific heat at low temperatures, the C_{44} value for natural graphite was estimated to be 0.23×10^{11} dyn/cm^2 by Bowman and Krumhansl,[51] and 0.405×10^{11} dyn/cm^2 and 0.452×10^{11} dyn/cm^2 by Komatsu.[23,24] Then, from the analysis of neutron scattering measurements, the C_{44} value at room temperature for HOPG was deduced to be $(0.42\pm 0.2) \times 10^{11}$ dyn/cm^2 by Dolling and Brockhouse[9] and $(0.46 \pm 0.02)\times 10^{11}$ dyn/cm^2 by Nicklow *et al.*[11] Thus, the C_{44} value at room temperature has not yet been determined unambiguously. As stated in Sec. VI, we determine from the analysis of the specific heat at low temperatures that the intrinsic C_{44} value at room temperature is 0.425×10^{11} dyn/cm^2.

Gauster and Fritz measured changes of ultrasonic transit times in HOPG as a function of temperature between 4 and 300 K and calculated the temperature dependence of five elastic constants C_{ij}.[52] Hwang measured sound velocities along the c axis of HOPG between 4 and 325 K with an ultrasonic pulse-echo phase comparison method and determined the temperature dependence of C_{33} with considerable accuracy.[53] On the other hand, Roy measured the temperature dependence of the longitudinal phonon frequency, propagating along the c axis, in pyrolytic graphite with a mosaic spread of approximately 10° by neutron scattering over a temperature range of 190 to 890 K.[54] The measured phonons correspond to $q_a = 0$, $q_z = q_z^{\max}$, and $\omega = \omega_z'$ of the out-of-plane mode in the present model, where $q_a^2 = q_x^2 + q_y^2$ and $q_z^{\max} = \pi/c$. From this measurement we obtain C_{33} through Eqs. (3), (7), and (13). Brockhouse and Shirane measured the temperature dependence of longitudinal and transverse phonons along or near the c axis between 4 K and 1500 °C on HOPG of mosaic spread $\sim 0.8°$.[55] The latter transverse phonons correspond to $q_a = 0$, $q_z = q_z^{\max}$, and $\omega = \omega_z$ of the present in-plane mode and give C_{44} through Eqs. (1) or (2), (6), and (10). Then, Ross measured the longitudinal phonons along the c axis on polycrystalline graphite at temperatures up to 1920 °C.[56]

Based on the above several measurements, we have determined the relative temperature dependence of C_{33}.

$0 \leqslant T \leqslant 146$ K:

$$\frac{C_{33}(T)}{C_{33}(0)} = f(T) = 1.0 - 6.50\times 10^{-7} T^2, \tag{15}$$

$146 \leqslant T \leqslant 1800$ K:

$$\frac{C_{33}(T)}{C_{33}(0)} = f(T) = 1.0145 - 1.990\times 10^{-4} T + 3.20\times 10^{-8} T^2, \tag{16}$$

TABLE I. Physical constants of graphite at room temperature.

C_{11}	106×10^{11} [a]	dyn/cm^2
C_{12}	18×10^{11} [a]	dyn/cm^2
C_{13}	1.5×10^{11} [a]	dyn/cm^2
C_{33}	3.65×10^{11} [a]	dyn/cm^2
C_{44}	0.425×10^{11} [b]	dyn/cm^2
κ	3.13×10^{-3} [b]	cm^2/s
c	3.3544×10^{-8}	cm
ρ	2.26	g/cm^3
V	5.30	cm^3/mol
v_l	2.16×10^{6} [c]	cm/s
v_t	1.40×10^{6} [d]	cm/s
ζ	1.88×10^{10} [e]	cm^2/s^2
μ	1.20×10^{13} [f]	s^{-1}
ω_z	8.18×10^{12} [g]	rad/s
ω_z'	2.40×10^{13} [h]	rad/s
K	2.80×10^{-12} [i]	cm^2/dyn

[a] Reference 47.
[b] Present analysis.
[c] Equation (4).
[d] Equation (5).
[e] Equation (6).
[f] Equation(7).
[g] Equation(10).
[h] Equation(13).
[i] Equation(37).

where T is the temperature.

The neutron scattering result shows that the relative temperature dependence of C_{44} is nearly the same as that of C_{33}.[55] Hence, we assume that

$$\frac{C_{44}(T)}{C_{44}(0)} = f(T). \tag{17}$$

The measurement of ultrasonic transit times indicates that the relative changes in C_{11} and C_{12} as a function of temperature are about $\frac{1}{2}$ of that in C_{33}.[52] The relative temperature dependence of C_{13} is not clear, but it is probably intermediate between that of C_{33} and that of C_{11} and C_{12}. Since $C_{11} \gg C_{13}^2/C_{33}$ in Eq. (4), the temperature dependence of C_{13} has only a negligible effect on this analysis. Here, we assume conservatively that the relative temperature dependence of C_{13} is the same as that of C_{11} and C_{12}. Therefore, we assume that

$$\frac{C_{11}(T)}{C_{11}(0)} = \frac{C_{12}(T)}{C_{12}(0)} = \frac{C_{13}(T)}{C_{13}(0)} = \frac{1+f(T)}{2}. \tag{18}$$

Then, the elastic constants $C_{ij}(T)$ at a temperature T are given by using $C_{ij}(293)$ at 293 K as follows:

$$C_{ij}(T) = \begin{cases} C_{ij}(293)\left(\dfrac{f(T)}{0.959}\right) & \text{for } C_{33} \text{ and } C_{44}, \\[2ex] C_{ij}(293)\left(\dfrac{1+f(T)}{1.959}\right) & \text{for } C_{11},\ C_{12},\ \text{and } C_{13}. \end{cases} \tag{19}$$

The value of κ cannot be measured by using the conventional mechanical methods, but it can be estimated from the analysis of the specific heat. Komatsu and Nagamiya obtained a κ value of 3.83×10^{-3} cm^2/s from the specific heat above 250 K by assuming $C_{44}=0$.[1] Later, Komatsu obtained another κ of 6.11×10^{-3} cm^2/s from the specific heat between 15 and 60 K with a calculated C_{44}.[3] Komatsu has given no explanation for the adoption of two different κ values. We consider that κ varies with temperature. The relative change of κ as a function of temperature is not necessarily the same as that of C_{ij}. In the present analysis we assume κ as a parameter and determine its temperature dependence in Sec. VI by fitting the calculated specific heat values to the experimental ones. Table I gives the values at room temperature of the elastic constants and other physical quantities that are used in the improved semicontinuum model.

B. Thermal expansion

Bailey and Yates measured the thermal expansion coefficients in the c- and a-axes directions of HOPG between 20 and 270 K.[57] The thermal expansion coefficient in the a-axis direction α_a was about $\frac{1}{20}$ of that in the c-axis direction α_c over the whole temperature range of measurement. Therefore, as stated already, we neglect α_a and take account of α_c only.

The thermal expansion coefficient in the c-axis direction as a function of temperature, which was obtained by Bailey and Yates, is formulated as follows:

$0 \leqslant T \leqslant 80$ K:

$$\alpha_c(T) = 5.350 \times 10^{-9} T^2 - 3.755 \times 10^{-11} T^3, \tag{20}$$

$80 \leqslant T \leqslant 273$ K:

$$\alpha_c(T) = 2.4352 \times 10^{-7} T - 7.690 \times 10^{-10} T^2 + 8.875 \times 10^{-13} T^3. \tag{21}$$

These formulas agree with their experimental data with a precision of 1%.

The interlayer spacing in the c-axis direction c is derived by integrating the above thermal expansion coefficients, that is, $\alpha_c = (1/c)(dc/dT)$, and substituting the interlayer spacing values at 4.2 K (Ref. 58) and at room temperature[59] (in Å):

$0 \leqslant T \leqslant 80$ K:

$$c(T) = 3.3360 + 5.95 \times 10^{-9} T^3 - 3.13 \times 10^{-11} T^4, \tag{22}$$

$80 \leqslant T \leqslant 273$ K:

$$c(T) = 3.3355 + 4.061 \times 10^{-7} T^2 - 8.55 \times 10^{-10} T^3 + 7.65 \times 10^{-13} T^4. \tag{23}$$

The α_c and c above 273 K are derived by connecting Eqs. (21) and (23) with the corresponding data above room temperature, which were obtained by Nelson and Riley,[60] Steward and Cook,[61,62] and Morgan:[63]

$273 \leqslant T \leqslant 1000$ K:

$$\alpha_c(T)=2.723\times10^{-5}+3.32\times10^{-9}(T-273)-1.15\times10^{-12}(T-273)^2, \tag{24}$$

$$c(T)=3.3526+9.128\times10^{-5}(T-273)+6.81\times10^{-9}(T-273)^2-1.12\times10^{-12}(T-273)^3, \tag{25}$$

$1000\leqslant T\leqslant 2873$ K:

$$\alpha_c(T)=2.734\times10^{-5}+2.41\times10^{-9}(T-273)-1.09\times10^{-13}(T-273)^2, \tag{26}$$

$$c(T)=3.3527+9.166\times10^{-5}(T-273)+5.29\times10^{-9}(T-273)^2. \tag{27}$$

C. Debye frequency

1. In-plane modes

The Debye frequencies of the in-plane longitudinal and transverse modes $\omega_{D,i}$ $(i=l,t)$ are given by the following equation, which is derived either from Eqs. (8), (9), and (14), or from the total number of modes within the volume enclosed with $q_z=\pi/c$, $q_z=-\pi/c$, and the frequency surface $\omega=\omega_{D,i}$ in the wave vector space:

$$\frac{V}{4\pi c v_i^2}\left(\omega_{D,i}^2-\frac{1}{2}\omega_z^2\right)=N_0. \tag{28}$$

Here, V/c is independent of temperature. The temperature dependence of v_i and ω_z is as follows:

$$v_i=v_i(293)\left[\left(\frac{1+f(T)}{1.959}\right)\left(\frac{c(T)}{c(293)}\right)\right]^{1/2}, \tag{29}$$

$$\omega_z=\omega_z(293)\left[\left(\frac{f(T)}{0.959}\right)\left(\frac{c(293)}{c(T)}\right)\right]^{1/2}. \tag{30}$$

2. Out-of-plane mode

The Debye frequency of the out-of-plane mode $\omega_{D,c}$ is given by the following equation, which is derived either from Eqs. (11), (12), and (14), or from the total number of modes within the volume enclosed with $q_z=\pi/c$, $q_z=-\pi/c$, and the frequency surface $\omega=\omega_{D,c}$ in the wave vector space:

$$\frac{V}{4\pi\kappa c}\left[\frac{2}{\pi}E(m)\omega_{D,c}\left(1+\frac{\zeta^2}{4\kappa^2\omega_{D,c}^2}\right)^{1/2}-\frac{\zeta}{2\kappa}\right]=N_0, \tag{31}$$

where

$$m=\left(\frac{\omega_z'}{\omega_{D,c}}\right)^2\left(1+\frac{\zeta^2}{4\kappa^2\omega_{D,c}^2}\right)^{-1}$$

and

$$E(m)=\int_0^{\pi/2}(1-m\sin^2\phi)^{1/2}d\phi.$$

Then, since $m<1$, $E(m)$ is approximately given by[64]

$$E(m)=\frac{\pi}{2}\left(1-\frac{1}{4}m-\frac{3}{64}m^2-\frac{5}{256}m^3-\cdots\right).$$

The temperature dependence of ω_z' and ζ is given by

$$\omega_z'=\omega_z'(293)\left[\left(\frac{f(T)}{0.959}\right)\left(\frac{c(293)}{c(T)}\right)\right]^{1/2}, \tag{32}$$

$$\zeta=\zeta(293)\left(\frac{f(T)}{0.959}\right)\left(\frac{c(T)}{c(293)}\right). \tag{33}$$

In Eq. (31), not only $\omega_{D,c}$ but also κ is included as the unknown. To determine both $\omega_{D,c}$ and κ, another condition in addition to Eq. (31) is necessary. The condition we choose is that the calculated specific heat values agree with the experimental ones. The procedure to determine both $\omega_{D,c}$ and κ is stated in Sec. VI.

Since $\omega_{D,c}>\omega_z'>\zeta/2\kappa$, Eq. (31) is expressed approximately by

$$\frac{V}{4\pi\kappa c}\omega_{D,c}\approx N_0, \tag{34}$$

which is useful for estimation of $\omega_{D,c}$ and κ.

IV. CALCULATION OF SPECIFIC HEAT

The calculated specific heat which should be compared with the experimental specific heat at constant pressure is the sum of the lattice specific heat at constant volume, the C_p-C_v correction, and the electronic specific heat, where C_p-C_v is the difference between the specific heat at constant pressure and that at constant volume.

A. Lattice specific heat at constant volume

The lattice specific heat at constant volume C_v for each mode is calculated by using its respective frequency distribution function $D(\omega)$ and Debye frequency ω_D:[65]

$$C_v=k\int_0^{\omega_D}\left(\frac{\hbar\omega}{kT}\right)^2\frac{e^{\hbar\omega/kT}}{(e^{\hbar\omega/kT}-1)^2}D(\omega)d\omega, \tag{35}$$

where k is the Boltzmann constant and $\hbar$ is the Planck constant divided by 2π. The calculated C_v for the in-plane longitudinal, the in-plane transverse, and the out-of-plane mode will be referred to as C_l, C_t, and C_c, respectively.

B. C_p-C_v correction

The difference C_p-C_v can be obtained from general thermodynamical considerations as follows:[66]

$$C_p-C_v=\frac{\alpha_v^2VT}{K}, \tag{36}$$

where α_v is the coefficient of volume expansion and $\alpha_v \approx \alpha_c$ in the present model. The temperature dependence of α_c is given in Sec. III B. Then, K is the compressibility and is given by using the elastic compliances S_{ij}:

$$K = 2(S_{11}+S_{12})+S_{33}+4S_{13} = \frac{C_{11}+C_{12}+2C_{33}-4C_{13}}{(C_{11}+C_{12})C_{33}-2C_{13}^2}. \tag{37}$$

The temperature dependence of K and V is as follows:

$$K \approx K(293)\left(\frac{0.959}{f(T)}\right) \tag{38}$$

and

$$V = V(293)\left(\frac{c(T)}{c(293)}\right). \tag{39}$$

C. Electronic specific heat

From the specific heat measurement below 1.2 K of natural Madagascar graphite, van der Hoeven and Keesom deduced the electronic specific heat C_e of a pure single crystal of graphite [in μJ/(mol K)]:[67]

$$C_e = 13.8\ T. \tag{40}$$

Since it is difficult to deduce experimentally the electronic specific heat above 2 K, we calculate it from the density of states near the Fermi level in the electronic energy band. Using the density of states given by Wallace's three-dimensional band model,[68] Komatsu and Nagamiya calculated the electronic specific heat per mol:[1]

$$C_e = \frac{2N_0}{\sqrt{3}\pi^2}\left(\frac{\gamma_1}{\gamma_0^2}\right)\left[\frac{\pi^2}{3}k^2T + 5.41\left(\frac{\pi}{\gamma_1}\right)k^3T^2 + \frac{7\pi^4}{30}\left(\frac{3}{4\gamma_1^2}\right)k^4T^3 + \cdots\right], \tag{41}$$

where γ_0 is the resonance integral between nearest neighbors in the plane, and γ_1 is that between nearest neighbors in adjacent planes. Putting $\gamma_0 = 3.11$ eV and $\gamma_1 = 0.385$ eV ($\gamma_0^2/\gamma_1 \cong 25$ eV) (Ref. 69) into Eq. (41), we have [in μJ/(mol K)]

$$C_e = 11.0\ T(1 + 1.16\times10^{-3}T + 2.6\times10^{-7}T^2 + \cdots). \tag{42}$$

We combine the experimental result of Eq. (40) at low temperatures with the calculated temperature dependence in the bracket of Eq. (42), and assume that the electronic specific heat is given as a function of temperature as follows [in μJ/(mol K)]:

$$C_e = 13.8\ T(1 + 1.16\times10^{-3}T + 2.6\times10^{-7}T^2 + \cdots). \tag{43}$$

V. EVALUATION OF SPECIFIC HEAT DATA FOR SINGLE-CRYSTAL GRAPHITE

A considerable amount of experimental work has been done on the low-temperature specific heat of graphite.[25,67,70–76] The experimental results, however, have shown a significant difference between different types of graphite specimens, which differ in the degree of stacking faults, the crystallite size, and/or the impurity concentration. It has been established that, at low temperatures, the specific heat values of more imperfect graphites are larger than those of pure and structurally perfect graphite. On the other hand, at high temperatures above room temperature, there is no significant difference in the specific heat between different types of graphite specimens.[77–81]

We estimate the intrinsic specific heat proper to single-crystal graphite, viz. pure and structurally perfect graphite, which should be compared with the calculated specific heat in the present analysis. We have evaluated almost all the data reported in the literature and chosen the following data for estimation of the intrinsic specific heat.

(1) 0.4–2.0 K: Data on Madagascar natural graphite measured by van der Hoeven and Keesom.[67]

(2) 1.3–20 K: Data on Canadian natural graphite measured by DeSorbo and Nichols.[75]

(3) 9.7–17 K: Data on artificial polycrystalline graphite (pile graphite) measured by DeSorbo and Nichols.[75]

(4) 20–120 K: Data on Ceylon natural graphite measured by DeSorbo.[72]

(5) 40–300 K: Data on artificial polycrystalline graphite (Acheson graphite) measured by DeSorbo and Tyler.[70]

(6) 300–1800 K: JANAF Thermochemical Tables.[77]

In the temperature range between 0.4 and 300 K, first, we plot the experimental raw data in the C_p vs T plane, and draw a smooth curve so that it runs through the data points. Then, we subdivide the temperature range into several subranges. In each subrange we fit a polynomial in T to the smooth curve under the boundary conditions that not only the absolute values of the polynomials but also their first and second derivatives with respect to T are continuous at the boundaries between adjacent subranges. The choice of subranges and the curve fitting are tried by the trial-and-error method. Then, in the final stage of data evaluation and fitting, we refer to the result of the present analysis. The polynomials thus obtained are shown in Table II. The values of these polynomials are continuous at the boundaries between adjacent subranges with an accuracy of 0.1%, and their first and second derivatives are continuous with an accuracy of 1%.

In the temperature range between 300 and 1800 K, we adopt the specific heat data given in JANAF Thermochemical Tables.[77] They are not the experimental raw data, but already evaluated data at 100-K intervals. All the JANAF data for this temperature range can be expressed as a single polynomial in T of degree 4. The absolute value of this polynomial is continuous to the low-temperature one at 300 K. However, its first and second derivatives are not continuous to the low-temperature ones. Hence, we subdivide the tem-

TABLE II. Formulation of the experimental specific heat values for single-crystal graphite C_p in J/(mol K). $C_p = a_0 + a_1T + a_2T^2 + a_3T^3 + a_4T^4 + a_5T^5$, where T is the temperature in K and coefficients a_i are given below.

T (K)	a_0	a_1	a_2	a_3	a_4	a_5
0.4–1	0	$1.391\,49 \times 10^{-5}$	$-7.739\,68 \times 10^{-7}$	$3.003\,39 \times 10^{-5}$	$-2.472\,72 \times 10^{-6}$	0
1–3.5	$3.227\,46 \times 10^{-7}$	$1.359\,65 \times 10^{-5}$	$-1.848\,48 \times 10^{-6}$	$3.209\,28 \times 10^{-5}$	$-3.667\,11 \times 10^{-6}$	$2.055\,68 \times 10^{-7}$
3.5–12.5	$1.374\,72 \times 10^{-4}$	$-1.589\,26 \times 10^{-4}$	$8.764\,11 \times 10^{-5}$	$7.961\,00 \times 10^{-6}$	$-2.640\,28 \times 10^{-7}$	$4.538\,55 \times 10^{-9}$
12.5–18.5	$1.643\,68 \times 10^{-3}$	$-8.302\,03 \times 10^{-4}$	$2.041\,44 \times 10^{-4}$	$-1.903\,77 \times 10^{-6}$	$1.443\,04 \times 10^{-7}$	$-2.083\,33 \times 10^{-9}$
18.5–35	$-2.160\,46 \times 10^{-2}$	$4.723\,46 \times 10^{-3}$	$-3.168\,82 \times 10^{-4}$	$2.195\,73 \times 10^{-5}$	$-3.841\,43 \times 10^{-7}$	$2.368\,43 \times 10^{-9}$
35–65	$1.334\,96 \times 10^{-1}$	$-1.681\,93 \times 10^{-2}$	$8.829\,44 \times 10^{-4}$	$-1.152\,40 \times 10^{-5}$	$8.361\,37 \times 10^{-8}$	$-2.458\,65 \times 10^{-10}$
65–118	$-4.673\,27 \times 10^{-2}$	$-2.310\,51 \times 10^{-3}$	$4.173\,31 \times 10^{-4}$	$-4.074\,65 \times 10^{-6}$	$2.417\,36 \times 10^{-8}$	$-5.650\,08 \times 10^{-11}$
118–185	$-2.952\,47 \times 10^{-1}$	$1.047\,67 \times 10^{-2}$	$1.107\,14 \times 10^{-4}$	$-2.838\,16 \times 10^{-7}$	$1.252\,95 \times 10^{-9}$	$-2.975\,10 \times 10^{-12}$
185–222	$1.909\,460 \times 10^{1}$	$-4.763\,194 \times 10^{-1}$	$4.967\,278 \times 10^{-3}$	$-2.432\,463 \times 10^{-5}$	$6.021\,457 \times 10^{-8}$	$-6.017\,768 \times 10^{-11}$
222–300	$7.124\,04 \times 10^{-1}$	$-1.343\,72 \times 10^{-2}$	$2.842\,42 \times 10^{-4}$	$-5.924\,01 \times 10^{-7}$	$8.741\,20 \times 10^{-11}$	$6.682\,13 \times 10^{-13}$
300–510	$-3.526\,120 \times 10^{1}$	$4.752\,160 \times 10^{-1}$	$-2.282\,650 \times 10^{-3}$	$5.822\,490 \times 10^{-6}$	$-7.302\,880 \times 10^{-9}$	$3.572\,450 \times 10^{-12}$
510–620	$-1.446\,127 \times 10^{2}$	$1.158\,705 \times 10^{0}$	$-3.439\,530 \times 10^{-3}$	$5.104\,493 \times 10^{-6}$	$-3.671\,931 \times 10^{-9}$	$1.001\,007 \times 10^{-12}$
620–760	$2.699\,737 \times 10^{2}$	$-1.881\,706 \times 10^{0}$	$5.364\,635 \times 10^{-3}$	$-7.434\,892 \times 10^{-6}$	$5.067\,046 \times 10^{-9}$	$-1.364\,005 \times 10^{-12}$
760–1000	$-5.828\,411 \times 10^{1}$	$3.611\,088 \times 10^{-1}$	$-7.127\,680 \times 10^{-4}$	$7.347\,003 \times 10^{-7}$	$-3.836\,109 \times 10^{-10}$	$8.038\,670 \times 10^{-14}$
1000–1800	$5.752\,91 \times 10^{0}$	$2.655\,47 \times 10^{-2}$	$-1.292\,97 \times 10^{-5}$	$2.154\,89 \times 10^{-9}$	0	0

perature range into several subranges, and determine the polynomials fitted to the JANAF data in the respective subranges under the boundary conditions that both the values and the first and second derivatives of the polynomials are continuous to the low-temperature ones and between subranges. The polynomials obtained are shown in Table II. They fit the JANAF data at 100-K intervals with an accuracy of less than 0.6% and the continuity of their first and second derivatives is very satisfactory. However, because the data available for evaluation are scarce, the polynomials above 300 K have some ambiguity. In particular, the oscillatory behavior of the second derivatives seems to be artificial. We conclude that the intrinsic specific heat of single-crystal graphite is given by the polynomials of Table II, although the polynomials above 300 K are not so well established.

VI. DETERMINATION OF κ BY FITTING OF CALCULATED SPECIFIC HEAT VALUES TO EXPERIMENTAL ONES

As $\omega_{D,c}$ is related to κ in Eq. (31), the only unknown in the present analysis is κ. Practically, however, κ and $\omega_{D,c}$ are determined simultaneously. Then, as stated in Sec. III A, the value of C_{44} at room temperature $C_{44}(293)$ is uncertain, ranging from 0.013 to 0.46×10^{11} dyn/cm^2. Therefore, after assigning a trial value to $C_{44}(293)$, we determine κ and $\omega_{D,c}$. In the following, we assume that the experimental specific heat values are given by the polynomial formulas of Table II.

The procedure to determine both κ and $\omega_{D,c}$ is as follows. First, we estimate the approximate values of κ and $\omega_{D,c}$. In the low-temperature region, the calculated specific heat values is almost independent of $\omega_{D,c}$. Therefore, the approximate value of κ can be obtained by fitting the calculated specific heat values to the experimental ones only if a trial high value is assumed for $\omega_{D,c}$. Then, the approximate value of $\omega_{D,c}$ is determined using Eq. (34). We proceed from the low-temperature region to the high-temperature region with a step-by-step increase of temperature. In the high-temperature region, the approximate values of κ and $\omega_{D,c}$ are estimated from their low-temperature values and Eq. (34). Secondly, starting with the approximate values of κ and $\omega_{D,c}$, we determine the final values of κ and $\omega_{D,c}$ self-consistently under the two conditions such that Eq. (31) is satisfied and the calculated specific heat agrees with the experimental one.

Figure 1 shows the temperature dependence of κ with $C_{44}(293)$ as a parameter. In the temperature range above 50 K, the temperature dependence of κ is almost the same for different $C_{44}(293)$ values. Below 50 K, however, the temperature dependence of κ differs markedly for different $C_{44}(293)$ values. If $C_{44}(293)$ is smaller than 0.425×10^{11} dyn/cm^2, when the temperature approaches to absolute zero, κ increases rapidly. On the contrary, if $C_{44}(293)$ is larger than 0.425×10^{11} dyn/cm^2, κ decreases rapidly. Such a rapid change in κ near absolute zero cannot be accepted physically.[82] Thus, based on this specific heat analysis at low temperatures, we conclude unambiguously that $C_{44}(293)$ is 0.425×10^{11} dyn/cm^2.

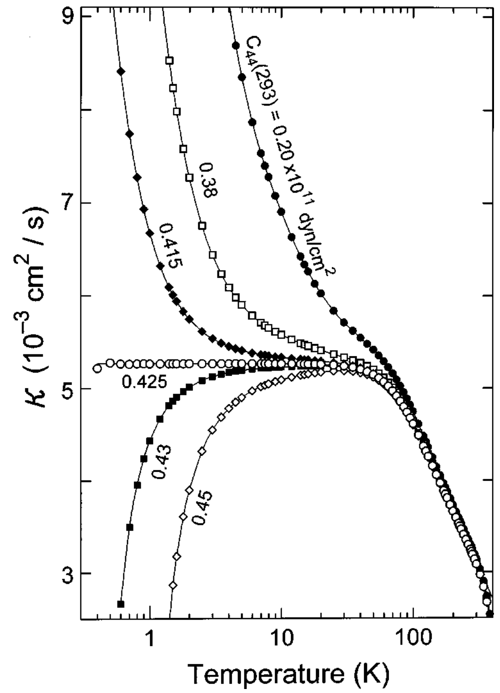

FIG. 1. Temperature dependence of κ. Parameters are C_{44} at room temperature.

The values of κ calculated with $C_{44}(293)=0.425\times10^{11}$ dyn/cm^2 are formulated as follows (in cm^2/s).

$0\leqslant T\leqslant 44.5$ K:

$$\kappa=5.265\times10^{-3}-9.45\times10^{-10}T^3, \tag{44}$$

$44.5\leqslant T\leqslant 120$ K:

$$\kappa=5.113\times10^{-3}+1.021\times10^{-5}T-2.290\times10^{-7}T^2+7.69\times10^{-10}T^3, \tag{45}$$

$T\geqslant 120$ K:

$$\kappa=1.0990\times10^{-2}-1.3830\times10^{-3}\ln T. \tag{46}$$

Above 50 K, the decreasing rate of κ with increasing temperature is much larger than that of C_{ij}.

The final calculation of the specific heat values is made by using the above formulas of κ. Tables III and IV show the calculated specific heat values, which are compared to the experimental ones given by the formulas of Table II. In the temperature range below 350 K, the calculated values agree with the experimental ones with an accuracy of less than 1%. Above 350 K, the calculated values become smaller than the experimental ones.

VII. DISCUSSION

A. Models of lattice vibrations and calculated results of specific heat

The usefulness of a lattice vibration model can be evaluated by comparing the calculated specific heat values by the

TABLE III. Calculated specific heat values of graphite for $0.4 \leqslant T \leqslant 10$ K. C_l, C_t, and C_c are the lattice specific heat at constant volume due to the in-plane longitudinal, the in-plane transverse, and the out-of-plane mode vibrations, respectively. Δ is the $C_p - C_v$ correction and C_e is the electronic specific heat. Observed values of C_p are from Table II.

T (K)	C_l [mJ/(mol K)]	C_t [mJ/(mol K)]	C_c [mJ/(mol K)]	Δ [mJ/(mol K)]	C_e [mJ/(mol K)]	Calculated C_p [mJ/(mol K)]	Observed C_p [mJ/(mol K)]
0.4	0.000 021	0.000 049	0.001 708	0.000 000	0.005 523	0.007 30	0.007 30
0.5	0.000 041	0.000 097	0.003 322	0.000 000	0.006 904	0.010 36	0.010 36
0.6	0.000 070	0.000 167	0.005 714	0.000 000	0.008 286	0.014 24	0.014 24
0.7	0.000 111	0.000 265	0.009 024	0.000 000	0.009 668	0.019 07	0.019 07
0.8	0.000 17	0.000 40	0.013 39	0.000 00	0.011 05	0.025 0	0.025 0
0.9	0.000 24	0.000 56	0.018 93	0.000 00	0.012 43	0.032 2	0.032 2
1.0	0.000 33	0.000 77	0.025 79	0.000 00	0.013 82	0.040 7	0.040 7
1.2	0.000 56	0.001 34	0.043 86	0.000 00	0.016 58	0.062 3	0.062 3
1.4	0.000 89	0.002 13	0.068 44	0.000 00	0.019 35	0.090 8	0.090 8
1.6	0.001 33	0.003 18	0.100 29	0.000 00	0.022 12	0.126 9	0.126 9
1.8	0.001 90	0.004 53	0.140 04	0.000 00	0.024 89	0.171 4	0.171 4
2.0	0.002 6	0.006 2	0.188 3	0.000 0	0.027 7	0.225	0.225
2.5	0.005 1	0.012 2	0.349 2	0.000 0	0.034 6	0.401	0.401
3.0	0.008 9	0.021 1	0.572 4	0.000 0	0.041 5	0.644	0.644
3.5	0.014 1	0.033 7	0.862 6	0.000 0	0.048 5	0.959	0.959
4.0	0.021 2	0.050 5	1.223 4	0.000 0	0.055 5	1.351	1.351
4.5	0.030 4	0.072 4	1.657 3	0.000 0	0.062 4	1.823	1.823
5.0	0.042	0.100	2.167	0.000	0.069	2.38	2.38
6.0	0.074	0.176	3.418	0.000	0.083	3.75	3.75
7.0	0.120	0.287	4.988	0.000	0.097	5.49	5.49
8.0	0.184	0.437	6.885	0.000	0.111	7.62	7.62
9.0	0.267	0.635	9.118	0.000	0.125	10.15	10.15
10.0	0.371	0.883	11.693	0.000	0.140	13.09	13.09

model with the experimental ones. Komatsu calculated the specific heat by using the semicontinuum model with C_{33}, C_{44}, and κ as adjustable parameters and could determine these parameters so as to fit the calculated values to the experimental ones for various kinds of graphite specimens below 20 K.[23,24] The value of C_{44} varied with the crystallite size or the degree of stacking faults of the specimens. Thus, the semicontinuum model, with the suitable choice of parameters, can well explain the specific heat below 20 K. As the temperature increases above 20 K, however, if the same parameters are used, the calculated specific heat values by the model deviate gradually from the experimental ones.

In the present paper, we have improved the semicontinuum model by taking the model parameters as a function of temperature. If we assume that the temperature dependence of κ is given by Eqs. (44)–(46), the improved semicontinuum model can explain the specific heat well in the temperature range below 350 K (Tables III and IV). The introduction of temperature dependence into the model parameters extends the temperature range in which the semicontinuum model is applicable from below 20 K to below 350 K. Thus, the improved semicontinuum model can be used more reliably below 350 K for the analysis of various physical properties than the previous model.

In the temperature range above 350 K, the calculated specific heat values by the improved semicontinuum model deviate gradually from the experimental ones. Namely, the model gives a valid approximation of lattice vibrations in the region of low frequencies and small wave vectors, but it becomes invalid for high frequencies or large wave vectors. A more rigorous model of lattice vibrations should be based upon the Born–von Kármán approach.[4–8,10–21]

Al-Jishi and Dresselhaus calculated the phonon-dispersion relations and the frequency distribution function by utilizing a Born–von Kármán model.[18] In their calculation, interactions up to fourth-nearest both intraplane and interplane neighbors were considered and the force constants were determined from the experimental data on Raman, infrared, and neutron scattering measurements and the measured elastic constants.[18] To calculate the frequency distribution function, the frequency range of 0–1650 cm^{-1} was divided into 165 intervals of width 10 cm^{-1} (i.e., about 1.88×10^{12} rad/s). We have calculated the specific heat by using their frequency distribution function. The width of intervals, however, is too broad to calculate accurately the specific heat at low temperatures below 50 K. In the temperature range from 50 to 1800 K, the calculated specific heat values agree with the experimental ones with a precision of about 2%.

B. Temperature dependence of lattice vibrations

1. Debye temperature

A conventional parameter to measure the temperature dependence of lattice vibrations is the Debye temperature Θ

TABLE IV. Calculated specific heat values of graphite for $10\leqslant T\leqslant 500$ K. Refer to the caption of Table III.

T (K)	C_l [J/(mol K)]	C_t [J/(mol K)]	C_c [J/(mol K)]	Δ [J/(mol K)]	C_e [J/(mol K)]	Calculated C_p [J/(mol K)]	Observed C_p [J/(mol K)]
10	0.000 371	0.000 883	0.011 693	0.000 000	0.000 140	0.013 09	0.013 09
12	0.000 65	0.001 54	0.017 90	0.000 00	0.000 17	0.020 3	0.020 3
14	0.001 02	0.002 42	0.025 60	0.000 00	0.000 20	0.029 2	0.029 2
16	0.001 48	0.003 51	0.034 88	0.000 00	0.000 22	0.040 1	0.040 1
18	0.002 03	0.004 82	0.045 85	0.000 01	0.000 25	0.053 0	0.053 0
20	0.002 66	0.006 33	0.058 61	0.000 01	0.000 28	0.067 9	0.067 9
25	0.004 60	0.010 95	0.098 64	0.000 04	0.000 36	0.114 6	0.114 6
30	0.007 03	0.016 75	0.149 86	0.000 09	0.000 43	0.174 2	0.174 1
35	0.009 9	0.023 7	0.210 6	0.000 2	0.000 5	0.245	0.245
40	0.013 3	0.031 7	0.278 9	0.000 3	0.000 6	0.325	0.325
45	0.017 1	0.040 8	0.352 9	0.000 5	0.000 7	0.412	0.412
50	0.021 4	0.051 0	0.431 2	0.000 7	0.000 7	0.505	0.505
55	0.026 2	0.062 4	0.513 0	0.001 1	0.000 8	0.603	0.603
60	0.031 4	0.074 8	0.597 7	0.001 5	0.000 9	0.706	0.706
65	0.037 1	0.088 2	0.685 0	0.001 9	0.001 0	0.813	0.813
70	0.043 2	0.102 8	0.774 7	0.002 4	0.001 0	0.924	0.924
75	0.049 8	0.118 5	0.866 7	0.003 0	0.001 1	1.039	1.039
80	0.056 8	0.135 3	0.961 2	0.003 5	0.001 2	1.158	1.158
85	0.064 3	0.153 1	1.058 0	0.004 1	0.001 3	1.281	1.281
90	0.072 3	0.172 0	1.157 2	0.004 7	0.001 4	1.408	1.408
95	0.080 7	0.192 0	1.258 9	0.005 3	0.001 5	1.538	1.538
100	0.089 6	0.213 2	1.363 0	0.006 0	0.001 5	1.673	1.673
110	0.108 7	0.258 7	1.578 3	0.007 5	0.001 7	1.955	1.955
120	0.130	0.309	1.802	0.009	0.002	2.25	2.25
130	0.152	0.363	2.033	0.011	0.002	2.56	2.56
140	0.177	0.422	2.270	0.013	0.002	2.88	2.88
150	0.204	0.485	2.512	0.014	0.002	3.22	3.22
160	0.232	0.552	2.758	0.016	0.003	3.56	3.56
170	0.262	0.624	3.007	0.018	0.003	3.92	3.92
180	0.295	0.701	3.257	0.020	0.003	4.28	4.28
190	0.329	0.781	3.507	0.022	0.003	4.64	4.64
200	0.365	0.866	3.754	0.024	0.003	5.01	5.01
210	0.402	0.954	3.997	0.026	0.004	5.38	5.38
220	0.442	1.046	4.234	0.028	0.004	5.75	5.75
230	0.483	1.142	4.465	0.030	0.004	6.12	6.13
240	0.527	1.241	4.687	0.032	0.004	6.49	6.49
250	0.572	1.343	4.901	0.034	0.005	6.85	6.86
260	0.619	1.448	5.105	0.036	0.005	7.21	7.21
270	0.668	1.556	5.299	0.038	0.005	7.57	7.57
280	0.719	1.665	5.483	0.039	0.005	7.91	7.92
290	0.771	1.777	5.656	0.041	0.005	8.25	8.26
300	0.826	1.889	5.820	0.042	0.006	8.58	8.60
320	0.939	2.118	6.118	0.045	0.006	9.23	9.27
340	1.060	2.349	6.380	0.048	0.007	9.84	9.93
360	1.186	2.580	6.609	0.051	0.007	10.43	10.58
380	1.318	2.809	6.808	0.054	0.008	11.00	11.23
400	1.455	3.034	6.982	0.057	0.008	11.54	11.87
450	1.813	3.573	7.323	0.064	0.010	12.78	13.38
500	2.187	4.068	7.566	0.071	0.011	13.90	14.70

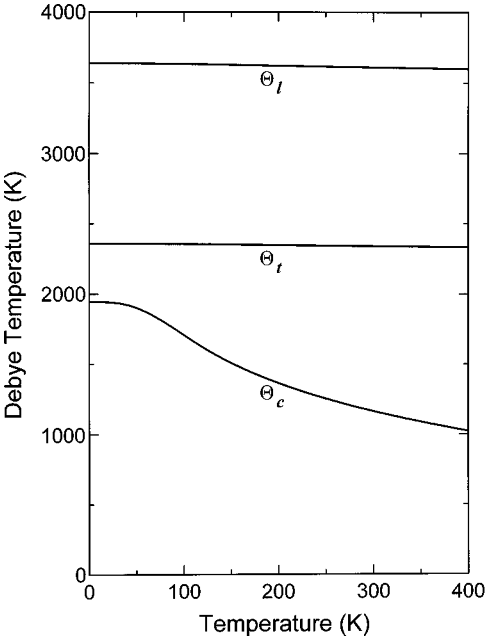

FIG. 2. Temperature dependence of Debye temperatures Θ_l, Θ_t, and Θ_c for in-plane longitudinal mode, in-plane transverse mode, and out-of-plane mode, respectively.

which is defined by $k\Theta = \hbar\omega_D$. Figure 2 shows the temperature dependence of the Debye temperatures for three vibrational modes. The Debye temperature of the out-of-plane mode decreases drastically with increasing temperature, which is related to the rapid decrease of κ.

2. Dispersion relation

Figures 3–7 show typical examples of the dispersion curves of lattice vibrations for $T=0$ and 293 K. The dispersion curves of the out-of-plane mode shown in Figs. 6 and 7 change remarkably with temperature, which is related to the rapid change of κ.

It is worth noting that the dispersion curves of the out-of-plane mode along the q_a direction shown in Fig. 6 are concave upwards. In usual cases, however, the geometry of the dispersion curves is such that they are convex upwards and tend to a horizontal tangent at the zone boundary, so that there is no three-phonon process in which all three phonons belong to the same polarization branch of lattice vibrations.[83] On the contrary, in the present case of graphite, as the dispersion curves are concave upwards, the three-phonon process in the out-of-plane branch can exist. The three-phonon process is important in analyzing the thermal conductivity.

Figure 8 shows the frequency distribution functions of three vibrational modes at 0 and 293 K. Figure 9 is the enlarged frequency distribution functions for the low frequency region of Fig. 8. A marked change in the frequency distribution function with temperature is shown clearly in the case of the out-of-plane mode.

3. Grüneisen constant

The Grüneisen constant γ is defined as the negative ratio of the relative frequency change $\Delta\omega/\omega$ to the relative volume change $\Delta V/V$, caused when the temperature T or pressure P is changed, i.e., $\gamma = -(\Delta\omega/\omega)/(\Delta V/V)$.

Table V compares the Grüneisen constants obtained by Raman scattering, neutron scattering, and the present analysis. For $\omega=\omega_z$ at $q_a=0$ and $q_z=q_z^{\max}$ of the in-plane longi-

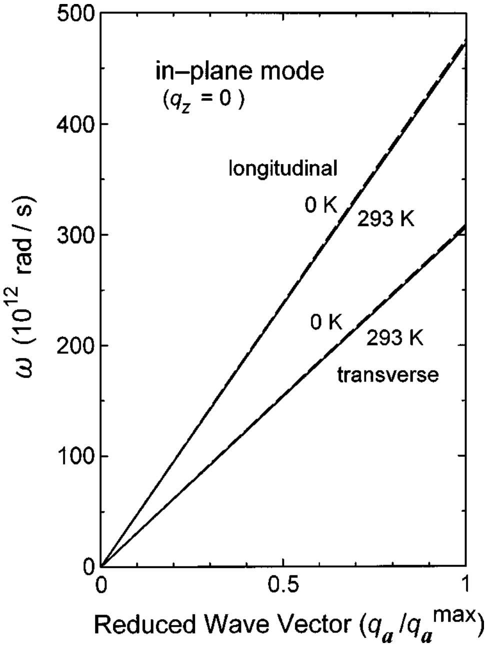

FIG. 3. Dispersion curves of the two in-plane modes along the q_a direction for $q_z=0$ at 0 and 293 K. $q_a^{\max}=4(\pi/3\sqrt{3})^{1/2}/a$ and a is the nearest neighbor atomic spacing. Effect of q_z on the curves is negligibly small except for near $q_a=0$.

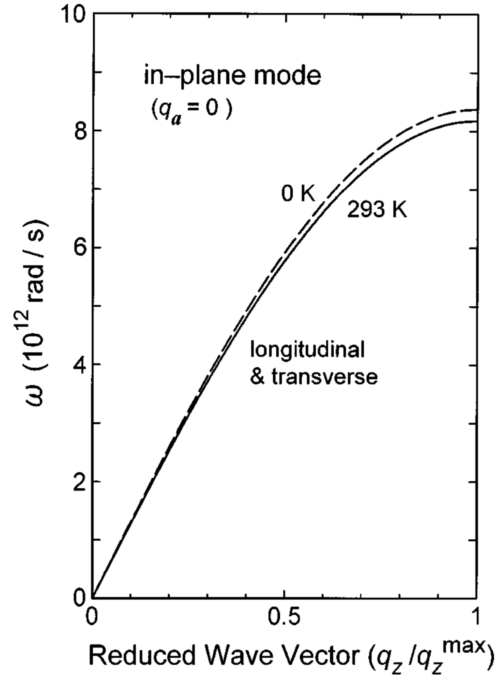

FIG. 4. Dispersion curves of the two in-plane modes along the q_z direction for $q_a=0$ at 0 and 293 K. $q_z^{\max}=\pi/c$ and c is the interlayer spacing.

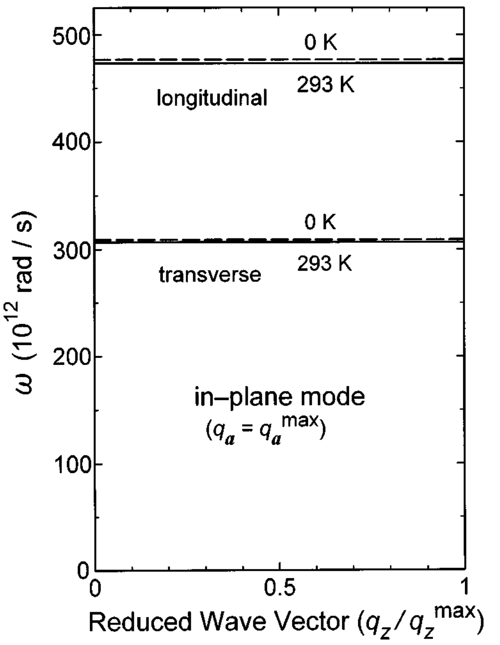

FIG. 5. Dispersion curves of the two in-plane modes along the q_z direction for $q_a=q_a^{\max}$ at 0 and 293 K.

tudinal and transverse modes and for $\omega=\omega_z'$ at $q_a=0$ and $q_z=q_z^{\max}$ of the out-of-plane mode, the experimental γ values agree rather well with the calculated ones.

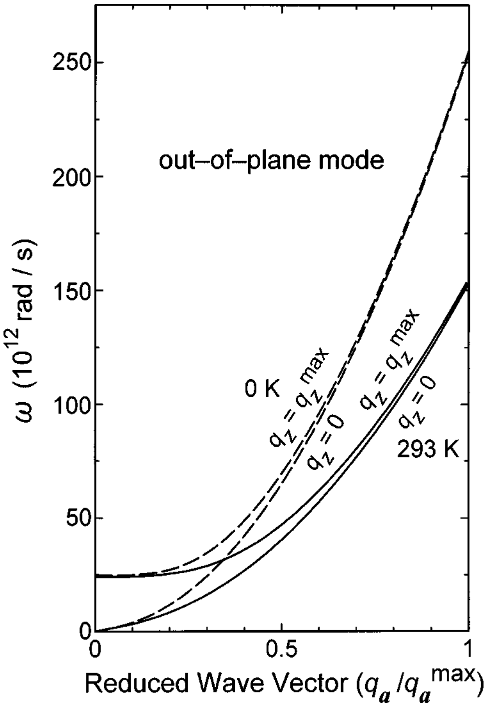

FIG. 6. Dispersion curves of the out-of-plane mode along the q_a direction for $q_z=0$ and $q_z=q_z^{\max}$ at 0 and 293 K.

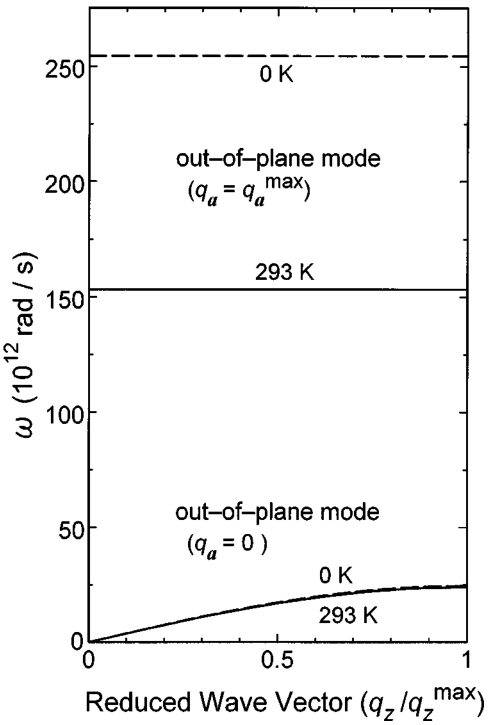

FIG. 7. Dispersion curves of the out-of-plane mode along the q_z direction for $q_a=0$ and $q_a=q_a^{\max}$ at 0 and 293 K.

For $\omega=\omega_{D,t}$ at $q_a=q_a^{\max}$ and $q_z=0$ of the in-plane transverse mode, the Raman scattering, $E_{2g}(2)$ at 1579 cm^{-1}, has given a low γ value of 0.10 under pressure, where $q_a^{\max}=4(\pi/3\sqrt{3})^{1/2}/a$ and a is the nearest neighbor atomic spacing in the layer plane. Hanfland *et al.* used $3\Delta a/a$ instead of $\Delta V/V$ so that they raised the γ value to 1.06.[84] Graphite is known to have negative thermal expansion coefficients parallel to the layer plane, i.e., $(3/a)(da/dT)<0$, below about 650 K.[59] Therefore, if we use $3\Delta a/a$ instead of $\Delta V/V$ in deriving γ by changing temperature, we will have a negative γ value.

Then, for $\omega=\omega_{D,c}$ at $q_a=q_a^{\max}$ and $q_z=0$ of the out-of-plane mode, the present analysis gives an extraordinarily large γ value of about 50, which is related to the rapid decrease of κ with temperature. There is no measurement of γ for this $\omega_{D,c}$, although Ivanov *et al.*[87] measured the pressure

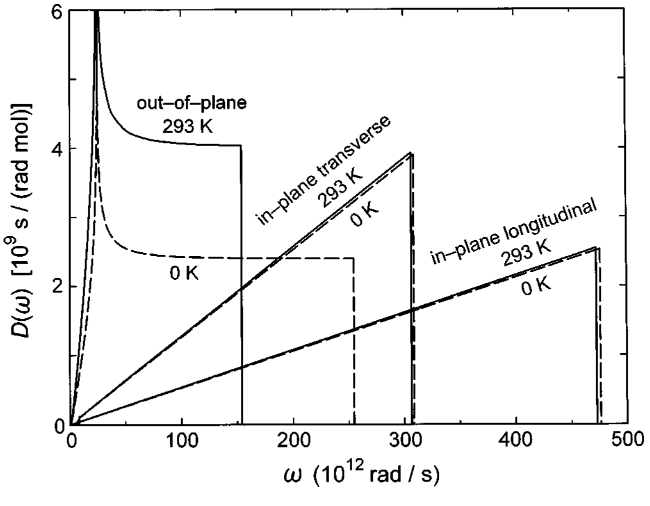

FIG. 8. Frequency distribution functions of in-plane longitudinal, in-plane transverse, and out-of-plane vibrations at 0 and 293 K.

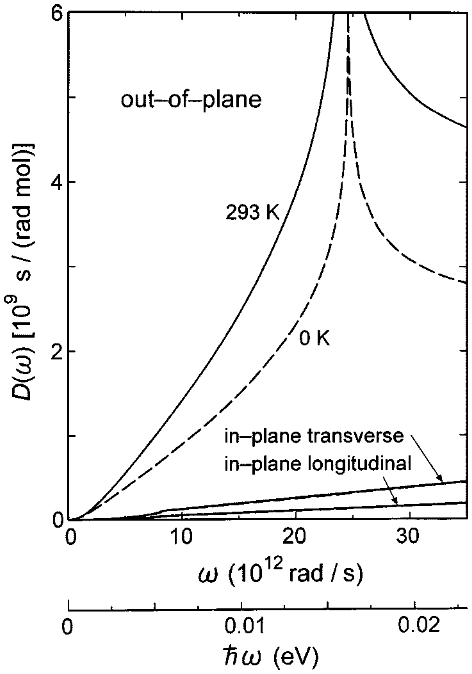

FIG. 9. Enlarged frequency distribution functions for the low frequency region.

dependence of the out-of-plane dispersion curve along the q_a axis for $q_a < 0.25 q_a^{\max}$ and $q_z = 0$, and found that ζ increases with pressure but κ decreases with it.

When the lattice specific heat at constant volume of the vibrational mode i is $C_{v,i}$ and the Grüneisen constant of the mode i is γ_i, if the average Grüneisen constant $\overline{\gamma}$ is defined by

$$\overline{\gamma} = \frac{\sum_i \gamma_i C_{v,i}}{\sum_i C_{v,i}} \quad \left(C_v = \sum_i C_{v,i} \right), \tag{47}$$

the following relation holds:[88]

$$\overline{\gamma} = \frac{\alpha_v V}{K C_v}. \tag{48}$$

Putting, at 293 K, $\alpha_v = 2.73 \times 10^{-5}$/K, $V = 5.30$ cm^3/mol, $K = 2.80 \times 10^{-12}$ cm^2/dyn, and $C_v = 8.30$ J/(mol K), we obtain $\overline{\gamma} \approx 0.62$ at 293 K. This $\overline{\gamma}$ value is smaller than the experimental γ values given in Table V, except the γ for $\omega = \omega_{D,t}$ of the in-plane transverse mode obtained by Raman scattering.

4. Temperature dependence of κ

The present analysis predicts that κ decreases rapidly with

TABLE V. Grüneisen constants γ in graphite. $q_a^2 = q_x^2 + q_y^2$, $q_a^{\max} = 4(\pi/3\sqrt{3})^{1/2}/a$ and $q_z^{\max} = \pi/c$, where a is the nearest neighbor atomic spacing and c is the interlayer spacing.

Vibrational mode	(q_a, q_z, ω)	Temp. (K)	Method	$\frac{1}{\omega}\frac{d\omega}{dT}$ (K^{-1})	$\frac{1}{V}\frac{dV}{dT}$ (K^{-1})	$\frac{1}{\omega}\frac{d\omega}{dP}$ (kbar^{-1})	$\frac{1}{V}\frac{dV}{dP}$ (kbar^{-1})	γ
In-plane longitudinal and transverse	$(0,\ q_z^{\max},\ \omega_z)$	300	Raman scattering[a]			1.10×10^{-2}	-2.96×10^{-3}	3.7
			Present analysis	-1.075×10^{-4}	2.73×10^{-5}			3.9
		296–1463	Neutron scattering[b]	-1.049×10^{-4}	2.88×10^{-5}			3.6
			Present analysis	-9.61×10^{-5}	2.88×10^{-5}			3.3
In-plane transverse	$(q_a^{\max},\ 0,\ \omega_{D,t})$	300	Raman scattering[a]			2.96×10^{-4}	-2.96×10^{-3}	0.10
			Present analysis	-3.23×10^{-5}	2.73×10^{-5}			1.2
Out-of-plane	$(0,\ q_z^{\max},\ \omega_z')$	190–296	Neutron scattering[c]	-1.236×10^{-4}	2.82×10^{-5}			4.4
			Present analysis	-1.080×10^{-4}	2.65×10^{-5}			4.1
		190–890	Neutron scattering[c]	-9.61×10^{-5}	2.81×10^{-5}			3.4
			Present analysis	-1.034×10^{-4}	2.79×10^{-5}			3.7
		4–1763	Neutron scattering[b]	-8.73×10^{-5}	2.74×10^{-5}			3.2
			Present analysis	-9.04×10^{-5}	2.74×10^{-5}			3.3
		293	Neutron scattering[d]			1.52×10^{-2}	-2.34×10^{-3}[e]	6.5
			Neutron scattering[f]			1.7×10^{-2}	-2.3×10^{-3}[e]	7.4
			Present analysis	-1.076×10^{-4}	2.73×10^{-5}			3.9
	$(q_a^{\max},\ 0,\ \omega_{D,c})$	293	Present analysis	-1.43×10^{-3}	2.73×10^{-5}			52

[a] Reference 84.
[b] Reference 55.
[c] Reference 54.
[d] Reference 85.
[e] This contains $(2/a)(da/dP) = -0.1 \times 10^{-3}$ kbar^{-1}, calculated from elastic constants.
[f] References 86 and 87.

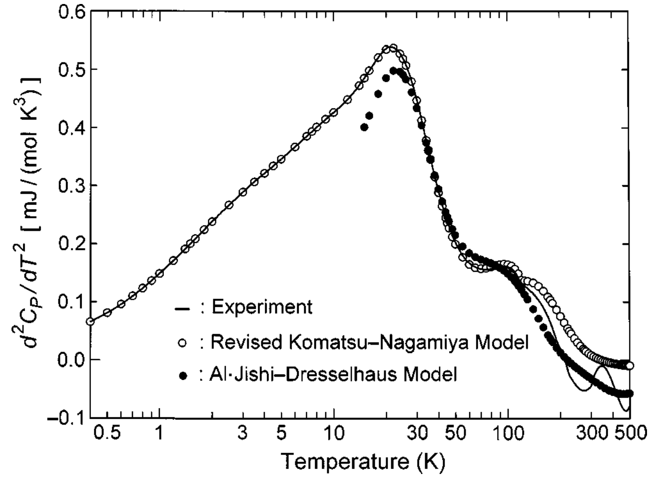

FIG. 10. Comparison of the experimental and the calculated second derivatives of the specific heat of graphite with respect to temperature.

increasing temperature; the bending elastic constant ofa-graphite layer decreases and the layers become easy to bend. In other words, the softening of the out-of-plane mode occurs such that the frequency of each out-of-plane mode decreases rapidly with temperature.

We suppose that the decrease of κ is related to the contraction of the a spacing in the layer planes. As previously mentioned, the a spacing decreases with increasing temperature below about 650 K, while the c spacing increases.[59] It is probable that the rapid increase in excitation of the out-of-plane vibrations with temperature results in the contraction of the a spacing.

The results of high-pressure experiments are suggestive in this respect. Both the c and a spacing decrease with pressure. Then, μ increases with pressure. Namely, $(1/c)(dc/dP) = -2.2\times10^{-3}/\text{kbar}$,[84–86] $(1/a)(da/dP) = -5\times10^{-5}/\text{kbar}$ (from elastic constants),[84] and $(1/\mu)(d\mu/dP) = 1.6\times10^{-2}/\text{kbar}$.[85–87] In the above measurement of the out-of-plane dispersion curve along the q_a axis, Ivanov *et al.* found that, although ζ increases with pressure, κ^2 decreases with it and drops to about 60% of its initial value at 60 kbar;[87] that is, $(1/\zeta)(d\zeta/dP) = 2.2\times10^{-2}/\text{kbar}$ and $(1/\kappa)(d\kappa/dP) = -3.8\times10^{-3}/\text{kbar}$. They considered that the decrease of κ with pressure is the precursor of the phase transition from graphite to hexagonal diamond at around 140 kbar.[89] These results suggest that the decrease of a spacing favors the decrease of κ, although the decrease of c spacing is against the decrease of κ.

We estimate the relation of κ to the a spacing under pressure and upon increasing the temperature. The above result of Ivanov *et al.* gives $(d\kappa/\kappa)/(da/a) = 7.6\times10^1$ under pressure. Then, when the temperature is increased at room temperature, we have $(d\kappa/\kappa)/(da/a) = 1.1\times10^3$, because $(1/\kappa)(d\kappa/dT) = -1.5\times10^{-3}/\text{K}$ from Eq. (46) and $(1/a)\times(da/dT) = -1.4\times10^{-6}/\text{K}$.[90] There is a difference of one order of magnitude in these estimates of $(d\kappa/\kappa)/(da/a)$. However, if we can exclude the effect of changes in the c spacing, the ratio of $d\kappa/\kappa$ to da/a may be approximately the same under pressure and upon increasing the temperature. This indicates that the decrease of κ is closely related to the contraction of the a spacing. The above difference may be due mainly to the fact that the c spacing decreases with pressure as $(dc/c)/(da/a) = 44$, whereas it increases with temperature as $(dc/c)/(da/a) = -20$. On the other hand, $(d\kappa/\kappa)/(dc/c) = 1.7$ under pressure, whereas $(d\kappa/\kappa)/(dc/c) = -55$ upon increasing the temperature; the two cases are in opposite directions to each other. Therefore, $d\kappa/\kappa$ has no direct relation to dc/c.

The predicted rapid decrease of κ with increasing temperature should be tested by such experiments as neutron scattering, electron energy loss spectroscopy (EELS), infrared reflection, and x-ray and neutron Bragg reflection. The neutron scattering experiment gives the dispersion relations directly as shown in Figs. 6 and 7. The surface phonon dispersion curves have been measured by using EELS.[91,92] As the measured surface phonon dispersion curves in graphite are in good agreement with the calculated bulk dispersion curves,[22] EELS is useful to test the temperature dependence of κ in the bulk. The infrared reflection observed at 868 cm^{-1} at room temperature has been identified as due to the A_{2u} out-of-plane mode,[93] which corresponds to $\omega = \omega_{D,c}$ at $q_a = q_a^{\max}$ and $q_z = 0$ of the out-of-plane mode in the present model. If the predicted temperature dependence of κ is valid, when the sample temperature is decreased from room temperature to 77 K, the frequency of the A_{2u} mode will shift to a higher frequency of about 50% increase. Then, the intensity of x-ray and neutron Bragg reflections depends on temperature and the frequency distribution function through the Debye-Waller factor.[65,94] The present analysis suggests that, except for the factor of the scattering vector, the intensity of the $(00l)$ reflection decreases more rapidly with increasing temperature than that of the $(hk0)$ reflection.

C. Second derivative of specific heat curve and frequency distribution function

The dispersion relations of lattice vibrations have been determined from neutron scattering experiments. Since the available flux of slow neutrons is limited, in practice the measurements are made in the range of $\omega < 1\times10^{14}$ rad/s, which is less than $\frac{1}{3}$ of the maximum frequency in the case of graphite. Then, Raman scattering and infrared measurements can probe only the optically active region of the wave vector space. On the contrary, the specific heat is unique in giving information integrating the whole wave vector space.

In the past the problem of "inversion" of specific heat curves was considered, in which the frequency distribution function $D(\omega)$ is calculated from the experimental specific heat curve.[44] The result, however, was not so fruitful, because the specific heat curve is remarkably insensitive to changes in $D(\omega)$. Here, we show that the second derivative of the specific heat curve with respect to temperature gives information on $D(\omega)$.

The second derivative of the specific heat at constant volume is derived from Eq. (35) as follows:

$$\frac{d^2C_v}{dT^2}=k\int_0^{\omega_D}\left[\frac{\partial^2E(T,\omega)}{\partial T^2}D(T,\omega)+2\,\frac{\partial E(T,\omega)}{\partial T}\,\frac{\partial D(T,\omega)}{\partial T}+E(T,\omega)\,\frac{\partial^2D(T,\omega)}{\partial T^2}\right]d\omega, \tag{49}$$

where

$$E(T,\omega)=\frac{z^2e^z}{(e^z-1)^2},\quad z=\frac{\hbar\omega}{kT},$$

$$\frac{\partial E(T,\omega)}{\partial T}=\frac{1}{T}\,\frac{z^2e^z}{(e^z-1)^3}[z+2+(z-2)e^z],$$

$$\frac{\partial^2E(T,\omega)}{\partial T^2}=\frac{1}{T^2}\,\frac{z^2e^z}{(e^z-1)^4}[z^2+6z+6+(4z^2-12)e^z+(z^2-6z+6)e^{2z}].$$

Figure 10 compares the experimental and the calculated results on the second derivative of the specific heat with respect to temperature. The experimental curve (solid line) is the second derivative of the formulas given in Table II. The calculated points (white and black circles) are derived by substituting $D(\omega)$ of the present revised semicontinuum model and that of Al-Jishi and Dresselhaus[18] into Eq. (49). In the calculation, the second derivatives of the C_p-C_v correction and the electronic specific heat are neglected. The calculated result for the revised semicontinuum model agrees well with the experimental curve below 120 K, but deviates gradually from it above 120 K. Then, for the Al-Jishi and Dresselhaus model, $D(\omega)$ is independent of temperature. As their calculated data points for $D(\omega)$ are scarce in the low frequency region, the calculation of the second derivatives is made above 15 K. The characteristics of $D(\omega)$ for both models are reflected on the respective second derivatives. Here, we do not discuss further the relation of the second derivatives and $D(\omega)$, but would like to emphasize that the second derivative of the specific heat curve with respect to temperature is useful in examining the validity of $D(\omega)$.

The second derivative of the experimental specific heat curve oscillates with temperature in the range of 300 to 760 K. We consider that the experimental curve is not good, because the integral of Eq. (49) becomes insensitive to the form of $D(\omega)$ at high temperatures and therefore the second derivative curve cannot oscillate rapidly with temperature. As stated in Sec. V, the oscillatory behavior of the second derivative in the range of 300 to 760 K seems to be artificial, which is due to the continuity condition of the first and second derivatives imposed in determining the experimental formulas of Table II. We recommend that the raw data of the specific heat above 300 K cited in the literature[77–81] should be reevaluated.

VIII. SUMMARY

The semicontinuum model of lattice vibrations in graphite proposed by Komatsu and Nagamiya has been improved by taking account of the temperature dependence of elastic constants and the thermal expansion. The specific heat proper to single-crystal graphite has been derived by evaluating the data reported in the literature. The bending elastic constant of a graphite layer has been determined by fitting the calculated specific heat to the experimental one. With the bending elastic constant thus determined, the improved semicontinuum model can explain the specific heat well in the temperature range below 350 K. Then, the bending elastic constant decreases more rapidly with increasing temperature than the other elastic constants, which means that softening of the out-of-plane vibrations occurs. It has been suggested that the softening of the out-of-plane vibrations with increasing temperature is closely related to the contraction of *a* spacing, i.e., the negative thermal expansion parallel to the layer planes. The Grüneisen constants have been calculated and compared with the experimental ones. The second derivative of the specific heat curve with respect to temperature gives information on the frequency distribution function of lattice vibrations. The value of C_{44} at room temperature has been determined to be 0.425×10^{11} dyn/cm^2.

ACKNOWLEDGMENT

We gratefully acknowledge discussions with Dr. A. Iwase of Japan Atomic Energy Research Institute.

---

*Present address: 513-3 Kuwada, Iwase-machi, Nishiibaraki-gun, Ibaraki-ken 309-1223, Japan.

†Present address: 1883-1 Toyooka, Tokai-mura, Naka-gun, Ibaraki-ken 319-1105, Japan.

[1] K. Komatsu and T. Nagamiya, J. Phys. Soc. Jpn. **6**, 438 (1951).

[2] T. Nagamiya and K. Komatsu, J. Chem. Phys. **22**, 1457 (1954).

[3] K. Komatsu, J. Phys. Soc. Jpn. **10**, 346 (1955).

[4] J. Krumhansl and H. Brooks, J. Chem. Phys. **21**, 1663 (1953).

[5] H. B. Rosenstock, J. Chem. Phys. **21**, 2064 (1953).

[6] A. Yoshimori and Y. Kitano, J. Phys. Soc. Jpn. **11**, 352 (1956).

[7] G. R. Baldock, Philos. Mag. **1**, 789 (1956).

[8] J. A. Young and J. U. Koppel, J. Chem. Phys. **42**, 357 (1965).

[9] G. Dolling and B. N. Brockhouse, Phys. Rev. **128**, 1120 (1962).

[10] H. Takahashi, Nucl. Sci. Eng. **37**, 198 (1969).

[11] R. Nicklow, N. Wakabayashi, and H. G. Smith, Phys. Rev. B **5**, 4951 (1972).

[12] A. A. Ahmadieh and H. A. Rafizadeh, Phys. Rev. B **7**, 4527 (1973).

[13] H. A. Rafizadeh, Physica (Amsterdam) **74**, 135 (1974).

[14] K. K. Mani and R. Ramani, Phys. Status Solidi B **61**, 659 (1974).

[15] A. P. P. Nicholson and D. J. Bacon, J. Phys. C **10**, 2295 (1977).

[16] R. J. Nemanich and S. A. Solin, Phys. Rev. B **20**, 392 (1979).

[17] M. Maeda, Y. Kuramoto, and C. Horie, J. Phys. Soc. Jpn. **47**, 337 (1979).

[18] R. Al-Jishi and G. Dresselhaus, Phys. Rev. B **26**, 4514 (1982).

[19] E. de Rouffignac, G. P. Alldredge, and F. W. de Wette, Phys. Rev. B **23**, 4208 (1981).

[20] G. P. Alldredge, E. de Rouffignac, B. Firey, and F. W. de Wette, Phys. Rev. B **29**, 3712 (1984).

[21] H. C. Gupta, J. Malhotra, N. Rani, and B. B. Tripathi, Phys. Rev. B **33**, 7285 (1986).

[22] G. Benedek and G. Onida, Phys. Rev. B **47**, 16 471 (1993).

[23] K. Komatsu, J. Phys. Chem. Solids **6**, 380 (1958).
[24] K. Komatsu, J. Phys. Chem. Solids **25**, 707 (1964).
[25] G. H. Wostenholm and B. Yates, Philos. Mag. **27**, 185 (1973).
[26] C. N. Hooker, A. R. Ubbelohde, and D. A. Young, Proc. R. Soc. London, Ser. A **284**, 17 (1965).
[27] B. Dreyfus and R. Maynard, J. Phys. (Paris) **28**, 955 (1967).
[28] B. T. Kelly, Carbon **5**, 247 (1967).
[29] B. T. Kelly, Philos. Mag. **15**, 1005 (1967).
[30] B. T. Kelly, Carbon **6**, 71 (1968).
[31] B. T. Kelly, Carbon **6**, 485 (1968).
[32] R. Taylor, B. T. Kelly, and K. E. Gilchrist, J. Phys. Chem. Solids **30**, 2251 (1969).
[33] T. Nihira and T. Iwata, J. Phys. Soc. Jpn. **49**, 1916 (1980).
[34] T. Nihira and T. Iwata, in *Point Defects and Defect Interactions in Metals*, edited by J. Takamura, M. Doyama, and M. Kiritani (University of Tokyo Press, Tokyo, 1982), p. 236.
[35] B. Nysten, J.-P. Issi, R. Barton, Jr., D. R. Boyington, and J. G. Lavin, Phys. Rev. B **44**, 2142 (1991).
[36] B. T. Kelly and P. L. Walker, Jr., Carbon **8**, 211 (1970).
[37] B. T. Kelly, J. Nucl. Mater. **24**, 210 (1967).
[38] B. T. Kelly, J. Nucl. Mater. **34**, 189 (1970).
[39] B. T. Kelly, Carbon **12**, 535 (1974).
[40] K. Sugihara and H. Sato, J. Phys. Soc. Jpn. **18**, 332 (1963).
[41] S. Ono and K. Sugihara, J. Phys. Soc. Jpn. **21**, 861 (1966).
[42] K. Sugihara, Phys. Rev. B **37**, 7063 (1988).
[43] K. Sugihara, Y. Hishiyama, and A. Ono, Phys. Rev. B **34**, 4298 (1986).
[44] M. Blackman, in *Handbuch der Physik*, edited by S. Flügge (Springer-Verlag, Berlin, 1955), Vol. 7, Pt. 1, pp. 325–382.
[45] J. de Launay, in *Solid State Physics*, edited by F. Seitz and D. Turnbull (Academic Press, New York, 1956), Vol. 2, pp. 219–303.
[46] N. W. Ashcroft and N. D. Mermin, *Solid State Physics* (Saunders College, Philadelphia, 1976), Chap. 23.
[47] O. L. Blakslee, D. G. Proctor, E. J. Seldin, G. B. Spence, and T. Weng, J. Appl. Phys. **41**, 3373 (1970).
[48] D. E. Soule and C. W. Nezbeda, J. Appl. Phys. **39**, 5122 (1968).
[49] C. Baker and A. Kelly, Philos. Mag. **9**, 927 (1964).
[50] E. J. Seldin and C. W. Nezbeda, J. Appl. Phys. **41**, 3389 (1970).
[51] J. C. Bowman and J. A. Krumhansl, J. Phys. Chem. Solids **6**, 367 (1958).
[52] W. B. Gauster and I. J. Fritz, J. Appl. Phys. **45**, 3309 (1974).
[53] D. M. Hwang, Solid State Commun. **46**, 177 (1983).
[54] A. P. Roy, Can. J. Phys. **49**, 277 (1971).
[55] B. N. Brockhouse and G. Shirane, Bull. Am. Phys. Soc. **17**, 123 (1972).
[56] D. K. Ross, J. Phys. C **6**, 3525 (1973).
[57] A. C. Bailey and B. Yates, J. Appl. Phys. **41**, 5088 (1970).
[58] Y. Baskin and L. Meyer, Phys. Rev. **100**, 544 (1955).
[59] B. T. Kelly, *Physics of Graphite* (Applied Science, London, 1981), Chaps. 1 and 4.
[60] J. B. Nelson and D. P. Riley, Proc. Phys. Soc. London **57**, 477 (1945).
[61] E. G. Steward and B. P. Cook, Nature (London) **185**, 78 (1960).
[62] E. G. Steward, B. P. Cook, and E. A. Kellett, Nature (London) **187**, 1015 (1960).
[63] W. C. Morgan, Carbon **10**, 73 (1972).
[64] L. M. Milne-Thomson, in *Handbook of Mathematical Functions*, edited by M. Abramowitz and I. A. Stegun (Dover Publications, New York, 1965), Chap. 17.
[65] J. M. Ziman, *Principles of the Theory of Solids* (Cambridge University Press, London, 1964), Chap. 2.
[66] C. Kittel, *Thermal Physics* (John Wiley & Sons, New York, 1969), Chap. 19.
[67] B. J. C. van der Hoeven, Jr. and P. H. Keesom, Phys. Rev. **130**, 1318 (1963).
[68] P. R. Wallace, Phys. Rev. **71**, 622 (1947). [Equation (5.3) and the density of electronic states $N(E)$ should be multiplied by 2π and $1/\pi$, respectively.]
[69] M. P. Sharma, L. G. Johnson, and J. W. McClure, Phys. Rev. B **9**, 2467 (1974).
[70] W. DeSorbo and W. W. Tyler, J. Chem. Phys. **21**, 1660 (1953).
[71] U. Bergenlid, R. W. Hill, F. J. Webb, and J. Wilks, Philos. Mag. **45**, 851 (1954).
[72] W. DeSorbo, J. Am. Chem. Soc. **77**, 4713 (1955).
[73] P. H. Keesom and N. Pearlman, Phys. Rev. **99**, 1119 (1955).
[74] W. DeSorbo and W. W. Tyler, J. Chem. Phys. **26**, 244 (1957).
[75] W. DeSorbo and G. E. Nichols, J. Phys. Chem. Solids **6**, 352 (1958).
[76] B. J. C. van der Hoeven, Jr., P. H. Keesom, J. W. McClure, and G. Wagoner, Phys. Rev. **152**, 796 (1966).
[77] D. R. Stull and H. Prophet, Natl. Stand. Ref. Data Ser. (U.S., Natl. Bur. Stand.) **37**, 1141 (1971).
[78] H. M. Spencer, Ind. Eng. Chem. **40**, 2152 (1948).
[79] R. E. Nightingale, H. H. Yoshikawa, and H. H. W. Losty, in *Nuclear Graphite*, edited by R. E. Nightingale (Academic Press, New York, 1962), Chap. 6.
[80] R. A. McDonald, J. Chem. Eng. Data **10**, 243 (1965).
[81] E. D. West and S. Ishihara, in *Advances in Thermophysical Properties at Extreme Temperatures and Pressures*, edited by S. Gratch (American Society of Mechanical Engineering, New York, 1965), pp. 146–151.
[82] J. A. Garber and A. V. Granato, Phys. Rev. B **11**, 3990 (1975).
[83] J. M. Ziman, *Electrons and Phonons* (Oxford University Press, London, 1960), Chap. 3.
[84] M. Hanfland, H. Beister, and K. Syassen, Phys. Rev. B **39**, 12 598 (1989).
[85] B. Alzyab, C. H. Perry, C. Zahopoulos, O. A. Pringle, and R. M. Nicklow, Phys. Rev. B **38**, 1544 (1988).
[86] A. S. Ivanov, A. V. Borman, V. P. Glazkov, I. N. Goncharenko, and V. A. Somenkov, Phys. Solid State **36**, 1656 (1994).
[87] A. S. Ivanov, I. N. Goncharenko, V. A. Somenkov, and M. Braden, Physica B **213 & 214**, 1031 (1995).
[88] M. Born and K. Huang, *Dynamical Theory of Crystal Lattices* (Oxford University Press, London, 1954), Chap. 2.
[89] F. P. Bundy and J. S. Kasper, J. Chem. Phys. **46**, 3437 (1967).
[90] E. A. Kellett and B. P. Richards, J. Nucl. Mater. **12**, 184 (1964).
[91] J. L. Wilkes, R. E. Palmer, and R. F. Willis, J. Electron Spectrosc. Relat. Phenom. **44**, 355 (1987).
[92] C. Oshima, T. Aizawa, R. Souda, Y. Ishizawa, and Y. Sumiyoshi, Solid State Commun. **65**, 1601 (1988).
[93] R. J. Nemanich, G. Lucovsky, and S. A. Solin, Mater. Sci. Eng. **31**, 157 (1977).
[94] R. M. Nicklow and R. A. Young, Phys. Rev. **152**, 591 (1966).